Intrinsic Flame Instabilities in Premixed and Nonpremixed Combustion

Moshe Matalon

McCormick School of Engineering and Applied Science, Northwestern University, Evanston, Illinois 60208-3125; email: matalon@northwestern.edu

Annu. Rev. Fluid Mech. 2007. 39:163–91

The *Annual Review of Fluid Mechanics* is online at fluid.annualreviews.org

This article's doi:
10.1146/annurev.fluid.38.050304.092153

0066-4189/07/0115-0163$20.00

Key Words

diffusive-thermal instability, hydrodynamic instability, large-scale explosions, cellular flames, flame oscillation, premixed flames, diffusion flames, edge-flames

Abstract

The focus of this article is on intrinsic combustion instabilities in both premixed and nonpremixed systems, identifying, in particular, the roles of differential and preferential diffusion, thermal expansion, and heat losses. For premixed flames, the hydrodynamic instability resulting from thermal expansion plays a central role and is particularly dominant in large-scale flames. It is responsible for the formation of sharp folds and creases in the flame front and for the wrinkling observed over the surface of expanding flames. In contrast, instabilities in diffusion flames, which give rise to cellular and oscillating flames, are mainly driven by diffusive-thermal effects, with thermal expansion playing a secondary role. The discussion also includes instabilities of edge-flames in unmixed reactants, which possess stability characteristics of both premixed and diffusion flames, but with a distinct mode of instability.

1. INTRODUCTION

Flame instability appears in different forms and at different scales. Spontaneous oscillations of an otherwise stable jet diffusion flame occur when the fuel concentration increases and the whole flame expands and contracts at a frequency of a few Hertz (Füri et al. 2000). A nominally planar flame in an upward uniform flow of a combustible mixture takes on a cellular appearance when varying the mixture composition, with cells of 0.5–1 cm in size (Markstein 1964). The surface of a large expanding flame, of magnitude 5–10 m in diameter, becomes spontaneously rough when it reaches a critical size and takes on a pebbled appearance with small ripples of approximately 10–50 cm covering its surface (Lind & Whitson 1977). Sustained pressure fluctuations of acoustic nature are observed in combustion chambers where unsteady combustion occurs. When occurring in practical systems these instabilities can be detrimental. For example, they can create conditions that may cause damage and mechanical failure to the combustion device. In other situations, however, they may be favorable for enhancing mixing and increasing burning rates.

This article focuses on intrinsic instabilities associated with the combustion process itself that would result even if there were no surrounding with which the combustion interacts. The subject has been covered at different depth in several articles that appeared in this series (Buckmaster 1993, Clavin 1994, Sivashinsky 1983), and this review attempts to complement these, focusing on topics not previously discussed or where significant progress has been made in physical understanding. References are only cited when directly relevant to the discussion, with no attempt to exhaustively cover all the literature on the subject. Insightful information obtained from computer simulations, for example, is not covered in depth and could be found in a recent review by Kadowaki & Hasegawa (2005).

Combustion processes are usually classified as premixed or nonpremixed, depending on whether the fuel and oxidizer are well mixed initially or are supplied from different origins. One section in this article is concerned with premixed flames. Although diffusive-thermal instabilities leading to cellular, polyhedral, and other multidimensional patterns are briefly mentioned, the focus is on the hydrodynamic instability resulting from thermal expansion, which has many ramifications in combustion. The second section in this article is concerned with nonpremixed combustion, in particular diffusion flame sheets and edge-flames in initially unmixed reactants. Thermal expansion does not play a crucial role in flame stability as it does in premixed flames. Cellular structures, oscillations, and other competing modes of instabilities are primarily driven by diffusive-thermal effects. Therefore, stability results are primarily discussed within the context of a constant-density approximation. When density variations are accounted for, these results are only slightly modified with thermal expansion acting to further stabilize or destabilize the flame depending on the mode of instability. The distinction between premixed and diffusion flames is not always retained in reality. In practical systems, where the fuel and oxidizer are supplied in two separate streams, it is often advantageous to run at high flow rates and stabilize the flame further downstream within the jet. Lifting the flame base off the burner has the advantage of avoiding thermal contact between the flame and the rim and

enhancing mixing in the dead space. The disadvantage is that the resulting edge-flame is subjected to instabilities and possible blow off. Stability results have so far been based on a constant-density model. The primary mode is oscillations, but unlike diffusion flames, which oscillate in a direction normal to the reaction sheet, an edge-flame moves back and forth along the stoichiometric surface and the oscillations decay further downstream along the trailing diffusion flame.

2. PREMIXED COMBUSTION

2.1. The Darrieus-Landau Instability

In purely theoretical analysis, Darrieus (1938) and Landau (1944) predicted independently that planar deflagrations are unconditionally unstable. This result was published nearly 65 years ago despite the fact that stable planar laminar flames have been observed in the laboratory since the pioneering work of Mallard & le Chatelier (1883). The Darrieus-Landau (DL) theory assumes that the flame is infinitesimally thin and propagates normal to itself at a constant speed S_L relative to the cold unburnt gas, unaffected by hydrodynamic disturbances. Within this framework, the linear stability of a planar flame yields

$$\omega = S_L k\, \omega_{DL}, \quad \omega_{DL} \equiv \frac{-\sigma + \sqrt{\sigma^3 + \sigma^2 - \sigma}}{\sigma + 1}, \tag{1}$$

where ω is the growth rate, k is the transverse wave number, and $\sigma \equiv \rho_u/\rho_b$ is the unburnt-to-burnt density ratio, or thermal expansion parameter. For exothermic chemical reactions $\sigma > 1$, the growth rate $\omega > 0$ for all wave number k, resulting in instability. The DL result, also known as the hydrodynamic instability, is a consequence of the gas thermal expansion. Indeed, ω increases with increasing σ and vanishes as $\sigma \to 1$. From Equation 1 we also see that ω is proportional to the wave number k, implying that wrinkles of short wavelength grow faster than wrinkles of long wavelength. This result, however, is not valid for short wavelength disturbances that are comparable to the flame thickness, because these may induce distortions of the flame structure that were not accounted for in the DL description. Diffusion processes within the flame often have stabilizing influences that may overcome the destabilizing effect of thermal expansion. For example, the surface of an outwardly propagating lean butane-air flame remains spherical and smooth in the early stages of propagation. This is in sharp contrast to a lean hydrogen-air flame, which at a comparable time appears inherently unstable (Strehlow 1984, pp. 428–29). In large-scale flames, however, the hydrodynamic instability is always present. It is responsible for the roughened surface observed on the surface of expanding flames and for the continuous wrinkling of the flame surface (Strehlow 1984, p. 432). The formation of multiple sharp crests pointing toward the burnt gas for flames attached to burners (Uberoi et al. 1958) and the sharp folds and creases observed on the surface of premixed flames in low-intensity turbulent flows (Sattler et al. 2002) are additional manifestations of the hydrodynamic instability.

The DL result can be easily extended to account for gravitational forces (Landau 1944). In this case, the dispersion relation yields

$$\omega = \frac{-\sigma + \sqrt{(\sigma^3 + \sigma^2 - \sigma) - (\sigma^2 - 1)(g/S_L^2 k)}}{\sigma + 1} S_L k,$$

where g is the gravitational acceleration. For a planar flame in an upward uniform flow, corresponding to downward propagation ($g > 0$), disturbances with wavelength $\lambda > 2\pi\sigma S_L^2/g$ are damped out by gravitational forces.[1] Gravity, therefore, acts to stabilize the long wavelength disturbances, and its influence is over a wider range of wavelengths for slow flames. Short wavelength disturbances, however, remain hydrodynamically unstable.

2.1.1. Hydrodynamic theory of flame propagation. A great deal of work has been done in the past 60 years to improve the DL model by incorporating the effects of the diffusion processes within the flame zone in the mathematical description. Notable is the study of Markstein (1964), who assumed a dependence of the flame speed on the local curvature of the front through a phenomenological constant that has become known as the Markstein length (or Markstein number, when expressed in units of the diffusion length). The more rigorous asymptotic treatment of Clavin & Williams (1982) and Matalon & Matkowsky (1982) exploits the multiscale nature of the problem characterized by two disparate length scales: the diffusion length l_f representing the flame thickness, where $l_f = \mathcal{D}_{th}/S_L$ with $\mathcal{D}_{th}$ the thermal diffusivity of the mixture, and the hydrodynamic length L associated, for example, with the average size of the wrinkles on the flame front or with the geometrical dimensions of the combustion vessel. The theory has since been extended to account for density variations, effects of differential and preferential diffusion with temperature-dependent transport coefficients, and effects due to stoichiometry and arbitrary reaction orders (Matalon et al. 2003).

Viewed on the hydrodynamic scale, the whole flame, where heat conduction, species diffusion, viscous dissipation, and chemical reactions occur, is considered a sheet separating the fresh combustible gases from the hot products. By resolving the internal flame structure on the much smaller diffusion scales, appropriate conditions for the velocities and pressure across the flame are obtained as matching conditions. In addition, an expression for the flame speed defined as the normal velocity of the unburnt gas relative to the sheet is obtained in the form

$$S_f = S_L - \mathcal{L}\,\mathbb{K},$$

where $\mathcal{L}$ is the Markstein length and $\mathbb{K}$ the flame stretch. Flame stretch is a measure of the flame front deformation resulting from its motion and nonuniformities in the underlying flow field, and in the present approximation it can be expressed as the sum of curvature κ and hydrodynamic strain $\mathbb{K}_s$, namely $\mathbb{K} = S_L\kappa + \mathbb{K}_s$ (Matalon 1983, Matalon et al. 2003). The dimensionless parameter $l_f\mathbb{K}/S_L$ is often referred to

[1]For upward propagation ($g < 0$), gravitational forces always act to further destabilize the flame.

as the Karlovitz number. The Markstein length is given by

$$\mathcal{L} = \left\{ \frac{\sigma}{\sigma - 1} \int_1^\sigma \frac{\lambda(x)}{x}\, \mathrm{d}x + \frac{\beta(Le_{\mathrm{eff}} - 1)}{2(\sigma - 1)} \int_1^\sigma \frac{\lambda(x)}{x} \ln\left(\frac{\sigma - 1}{x - 1}\right) \mathrm{d}x \right\} l_{\mathrm{f}},$$

where β is the Zel'dovich number, or activation energy parameter, Le_{eff} is the effective Lewis number of the mixture, and $\lambda = \lambda(T)$ is the thermal conductivity of the mixture, which depends solely on the temperature T. The effective Lewis number is a weighted average of the individual Lewis numbers Le_{F} and Le_{O} representing the ratios of the thermal diffusivity of the mixture to the mass diffusivities of the fuel and oxidizer, respectively. It depends on the equivalence ratio in such a way that for fuel-lean mixtures it reduces to Le_{F} and for fuel-rich mixtures to Le_{O}.

The resulting formulation is a nonlinear free-boundary problem supplemented with conditions that describe the influences of the diffusion processes occurring within the flame zone. The Markstein length, of the order of the flame thickness, is the only parameter in the model that depends on the mixture composition through the Lewis numbers. For hydrocarbon-air mixtures it is generally positive and decreases monotonically as the mixture varies from lean to rich conditions. The opposite is true for light fuels, such as hydrogen-air mixtures, where $\mathcal{L}$ decreases as the mixture varies from rich to lean conditions and may even be negative in sufficiently lean mixtures. Despite its relative simplicity, the hydrodynamic model exhibits a complex interaction between the flame and the surrounding gas. It was used in simple circumstances to examine the nature of the flow induced by thermal expansion, such as the displacement effect caused by the flame (Eteng et al. 1986), and was found particularly useful in studies aimed at examining the intricate nature of flame instabilities.

2.1.2. Planar flames. Reconsidering the linear stability of a planar flame, Pelce & Clavin (1982), Matalon & Matkowsky (1982, 1984), and Frankel & Sivashinsky (1982) derived a correction to the DL result of the form

$$\omega = S_{\mathrm{L}} k\, \omega_{\mathrm{DL}} - S_{\mathrm{L}} l_{\mathrm{f}} \left[B_1 + \beta(Le_{\mathrm{eff}} - 1) B_2 + \mathrm{Pr}\, B_3 \right] k^2,$$

that clarifies the role of diffusion on flame stability. Here Pr is the Prandtl number and the coefficients B_1, B_2, B_3, which depend solely on σ, are all positive. The three terms multiplying l_{f} correspond to thermal, molecular, and viscous diffusion, respectively. Thermal diffusion, which tends to smooth out temperature differences, always has a stabilizing influence. Due to the large change in viscosity across the flame, viscous diffusion also has a stabilizing influence.[2] On the other hand, the effect of molecular diffusion depends on the mixture composition, or the effective Lewis number of the mixture.

To ensure stabilization of the short wavelength disturbances Le_{eff} must exceed a critical value Le^*_{eff}. If long wavelength disturbances are excluded, because of the presence of walls in the transverse direction or as a result of the stabilizing influence of

[2] For a constant viscosity flow $B_3 = 0$; the role of viscosity is then secondary to that of thermal and molecular diffusion.

gravity, a stable planar flame results. For $Le_{\text{eff}} < Le^*_{\text{eff}}$, however, the short wavelength disturbances are also unstable and the hydrodynamic instability is enhanced by the diffusive effects. A planar flame under such circumstances cannot exist, a limit referred to as the diffusive-thermal instability. Proper description of the resulting cellular flame requires including higher-order terms in the dispersion relation (Equation 2.1) for short wave stabilization. This was explored for weak thermal expansion (Sivashinsky 1977) giving rise to a dispersion relation of the form

$$\omega = \frac{1}{2}(\sigma - 1)S_L k - \frac{1}{2}S_L l_f (Le_{\text{eff}} - Le^*_{\text{eff}})k^2 - 4\mathcal{D}_{\text{th}} l_f^2 k^4$$

with $Le^*_{\text{eff}} = 1 - 2\beta^{-1}$. The critical value Le^*_{eff} is slightly less than one, but when estimated from Equation 2.1 for realistic values of $\sigma \approx 6$ it is much lower, rarely exceeding 0.5. This makes most real combustion systems inaccessible to the instability except perhaps for lean hydrogen-air flames.

The critical Lewis number Le^*_{eff} increases when heat losses are incorporated in the analysis and approaches one near the flammability limit (Jackson & Kapila 1986, Joulin & Clavin 1979). All flames with $Le_{\text{eff}} \gtrapprox 1$ are then diffusively unstable at near extinction.

The constant-density theory identifies another form of instability, a pulsating mode, for mixtures with sufficiently large Lewis numbers (Sivashinsky 1983). Even when the hydrodynamically unstable long wavelength perturbations are suppressed, the predicted value of Le_{eff} for the onset of oscillations is quite large and not readily accessible for common combustible mixtures. The combined effects were recently discussed by Class et al. (2003). The critical Lewis number, however, is significantly reduced in the presence of heat losses, which explains the observed pulsations in burner stabilized flames (Blackshear et al. 1984).

2.2. Spherically Expanding Flames

The onset of cells on spherically expanding flames more clearly illustrates the distinction between the diffusive-thermal and hydrodynamic instabilities.

When a combustible mixture is centrally ignited, an outwardly propagating spherical flame develops. Due to the unsteady nature of the basic state, the stability analysis is not straightforward. First, the perturbed governing equations contain time-dependent coefficients and thus do not admit normal mode solutions with exponential growth. Furthermore, the notion of stability/instability must be accurately defined. Because the flame is expanding, one can only speak of the instantaneous growth rate, reflecting the tendency of the flame front toward stability or instability at a given moment. If at a given instant a disturbance increases but the flame grows even more rapidly, the disturbance appears to decay relative to the flame, thus implying stability. Instability results when the disturbance grows at a faster rate than the flame. If under certain conditions the flame is momentarily unstable for all times $t > t_c$, an instability results and will be observed in an experiment at a time larger than t_c.

A theoretical description of the onset of instability in a spherically expanding flame was given by Istratov & Librovich (1969), who considered a DL model with

a Markstein correction, and later by Bechtold & Matalon (1987), who, based on the hydrodynamic model, incorporated hydrodynamic and diffusive-thermal effects in a more systematic way. More recently, the results were generalized to allow for temperature-dependent transport coefficients and a wider range of equivalence ratios (Addabbo et al. 2002). Let the spherical flame be expressed by $r = R(t)$, the propagation speed $\dot{R}$, where the dot represents differentiation with respect to time, is deduced from Equation 2. The perturbed front can then be expressed in the form $r = R(t)\,[1 + A(t)\,\mathbb{S}_n(\theta, \varphi)]$, where A is the amplitude of the disturbance and $\mathbb{S}_n$ the spherical surface harmonics with n as an integer. The growth rate is then given by

$$\frac{1}{A}\frac{dA}{dt} = \frac{\dot{R}}{R}\left\{\tilde{\omega}_{\mathrm{DL}} - \frac{l_{\mathrm{f}}}{R}\left[\tilde{B}_1 + \beta(Le_{\mathrm{eff}} - 1)\tilde{B}_2 + \mathrm{Pr}\,\tilde{B}_3\right]\right\},$$

where the coefficients $\tilde{\omega}_{\mathrm{DL}}$ and $\tilde{B}_1, \tilde{B}_2, \tilde{B}_3$ depend only on σ and n, and with the exception of the low values of n they are all positive. Consistent with the hydrodynamic description, this result is valid for $R > R_0$ where R_0 is the initial flame radius, which is assumed larger than the diffusion length l_{f}. The first term $\tilde{\omega}_{\mathrm{DL}}$ represents the destabilizing effect of thermal expansion, whereas those multiplying l_{f} represent, respectively, the influences of thermal, molecular, and viscous diffusion.

When the right-hand side of Equation 5 is positive, which occurs when $Le_{\mathrm{eff}} < Le^*_{\mathrm{eff}}$, the amplitude grows in time for all n starting at $t = 0$. In this case, the instability, which must have developed when the flame radius was smaller than the initial radius R_0, is diffusive-thermal in nature. Indeed, spherically expanding flames in rich hydrocarbon-air or lean hydrogen-air mixtures, characterized by a Lewis number sufficiently less than one, were observed to take on a cellular appearance shortly after ignition (Manton et al. 1952, Palm-Leis & Strehow 1969).

When $Le_{\mathrm{eff}} > Le^*_{\mathrm{eff}}$, the right-hand side of Equation 5 for a given n changes sign only when the flame reaches the critical size $R = R_{\mathrm{c}}$. Thus, the amplitude decays initially, reaches a minimum at time $t = t_c$ corresponding to R_{c}, and then increases indefinitely in time. During the early stages of propagation the hydrodynamic instability is suppressed because of the large curvature of the front, and since for high Lewis numbers molecular diffusion exerts stabilizing influences on the short wavelength disturbances, a smooth (stable) flame results. Indeed, in lean hydrocarbon-air or rich hydrogen-air mixtures, the expanding flame remained smooth during the early stages of propagation, but took on a cellular appearance once it reached a critical size (Groff 1982, Simon & Wong 1953). In this case, the instability is hydrodynamic in nature, triggered by thermal expansion effects.

Figure 1 shows the development of spherically expanding hydrogen-air and propane-air flames for lean and rich mixtures at different pressures (Law 2006). The experiments were carried out in a spherical bomb, carefully designed to maintain a nearly constant pressure. At five atmospheres the rich propane-air ($\phi = 1.4$) and lean hydrogen-air ($\phi = 0.6$) flames are diffusively unstable because the effective Lewis number is below one in both cases. The instability seems to form shortly after ignition, namely when the flame size is sufficiently small and comparable to the flame thickness. In contrast, lean propane-air ($\phi = 0.7$) and rich hydrogen-air ($\phi = 4.0$) flames at five atmospheres remain stable for a significant time after ignition. Because

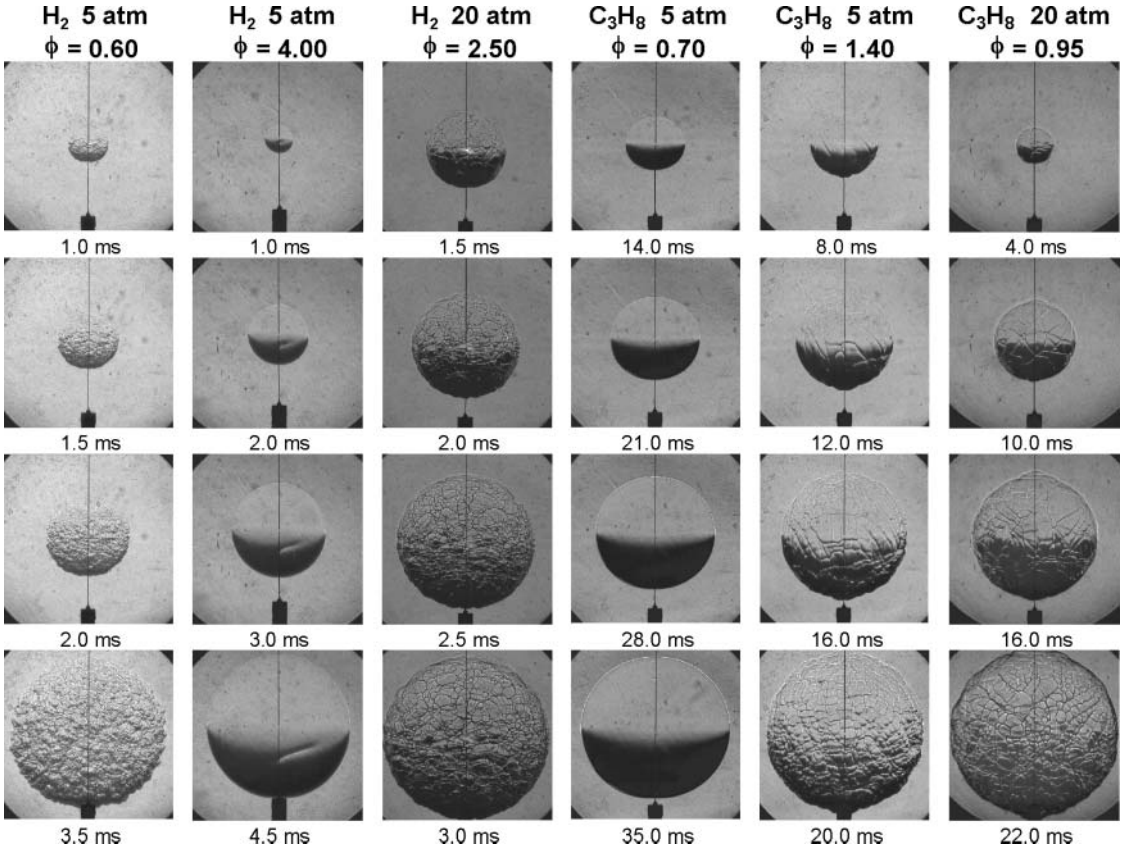

Figure 1

Observation of spherically expanding propane-air and hydrogen-air flames for various pressures and equivalence ratios ϕ. At 5 atm rich propane-air and lean hydrogen-air flames are diffusively unstable and take on a cellular appearance during the early stages of propagation; in contrast, lean propane-air and rich hydrogen-air flames are diffusively stable and their surface remains smooth for a sufficiently long time. The early wrinkling of lean propane-air and rich hydrogen-air flames at 20 atm is a consequence of the hydrodynamic instability. Courtesy of C.K. Law.

the effective Lewis number for such mixtures is sufficiently large, the flames are diffusively stable. However, at 20 atmospheres the lean propane-air ($\phi = 0.95$) and rich hydrogen-air ($\phi = 2.5$) flames become wrinkled early on during the propagation. At high pressure, the flame thickness l_f is significantly reduced and the stabilizing influences of diffusion are minimized. The wrinkling is therefore a direct consequence of the hydrodynamic instability.

Information about the range of cell size observed during the self-wrinkling phenomenon can be deduced from Equation 5 in the form of a marginal stability curve, as illustrated in **Figure 2**. The graph shows the range of unstable modes as a function of the Peclet number $\mathrm{Pe} = RS_L/\mathcal{D}_{th}$, or instantaneous flame size. The nose of

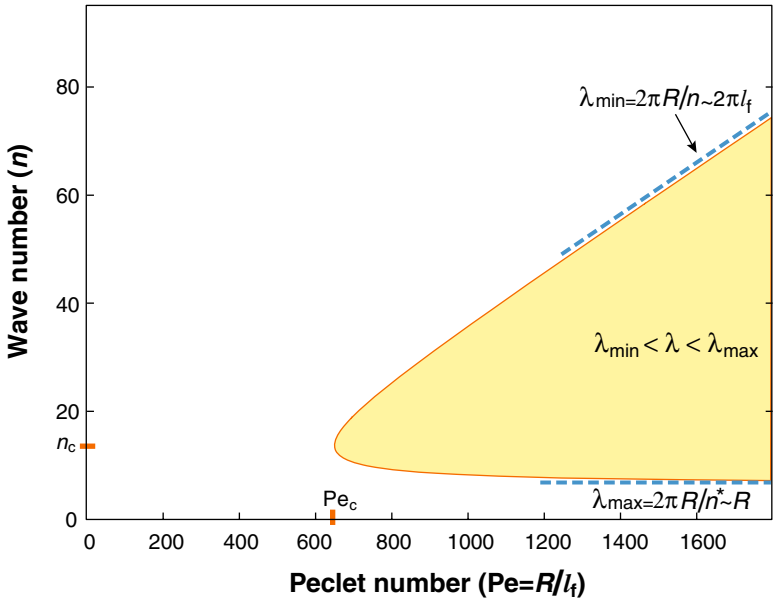

Figure 2

Peninsula of instability for spherically expanding flames. The graph shows the range of unstable modes for a given Peclet number Pe, or flame size R. Calculated for $Le_{\text{eff}} = 1.23$, $\text{Pr} = 0.7$, $\sigma = 6$, and $\lambda \sim T^{1/2}$.

the peninsular instability determines the critical Peclet number Pe_c, or critical radius R_c, when the flame first becomes unstable. At the onset of the instability the fastest-growing disturbance corresponds to $n_c \approx 14$, implying that the flame surface is instantaneously covered with a large number of cells. As the flame continues to expand, disturbances of spherical harmonics higher than n_c grow faster, suggesting that more and more cells develop on the flame surface. Expected cell sizes fall in the range $\lambda_{\text{min}} < \lambda < \lambda_{\text{max}}$ with larger corrugations stabilized by stretch and disturbances with shorter wavelength stabilized by diffusion. The lower branch of the peninsula very quickly asymptotes to the constant value n^* and because the stabilizing mechanism here is purely hydrodynamic, n^* depends only on σ; for realistic values of thermal expansion $n^* \approx 7$. This value determines the largest expected cell size, $\lambda_{\text{max}} = 2\pi R/n^*$, which increases with radius linearly: as the flame expands, the stretch rate decreases and cells of larger and larger size are able to develop on the flame surface. But large cells are extremely sensitive to external noise, which, when amplified by the hydrodynamic instability, leads to the spontaneous appearance of small-scale structures, or smaller-size cells, as discussed below. The upper branch of the peninsula asymptotes to a line, $Pe/n = C$, where the constant C depends on the Lewis number. Hence, the smallest cell size $\lambda_{\text{min}} = 2\pi R/n \sim 2\pi C\, l_f$ scales on the diffusion length and depends on the mixture composition. Because cells that are too small cannot survive, it is plausible to expect that λ_{min} is representative of the average cell size, when the whole flame surface becomes cellular.

Details of the transition from stable to cellular flames were recently studied by Bradley and coworkers (Bradley et al. 1998, 2000; Bradley & Harper 1994) and Law and coworkers (Jomaas et al. 2005, Law et al. 2005). Bradley's results indicate that the

theoretical predictions underestimate the critical Peclet number corresponding to the appearance of cells. Because of the unsteady nature of the problem, the initial growth of disturbances does not necessarily coincide with the time when the instability is first observed in an experiment. Disturbances that started growing at the time t_c may not be detected until their amplitude reaches a significantly larger size. Furthermore, when allowing for the dependence of the transport coefficients on temperature, and/or by accounting for radiation losses from the pocket of burnt gas, the onset of instability was delayed to larger values of Pe, yielding results that are more commensurate with the experimental record (Addabbo et al. 2002, Bechtold et al. 2004). This suggests that the instability threshold is sensitive to the physical parameters. The results of Law and coworkers show that a quantitative agreement between theory and experiment requires a sensible choice of flame properties that depend on the local experimental conditions. The evaluation of the thermal diffusivity of the mixture, for example, is subject to uncertainties in the choice of temperature and concentrations, as is the global activation energy, which additionally depends on the detailed reaction mechanism. With a judicious choice of the parameters, the predicted critical Peclet number was found to agree with the experimental conditions under a wide range of conditions (Jomaas et al. 2005). The experimental wave numbers, determined from cine and PLIF images of cells, fall within a peninsular of instability similar to that of **Figure 2** (Bradley et al. 2000), and the experimentally measured values of cell size, ranging from 6.5 to 10 mm, are in the same range of the predictions (Addabbo et al. 2002).

The self-wrinkling phenomenon of expanding flames gives rise to flame acceleration, with the flame radius increasing in time according to a power law, $R \sim t^a$, whose exponent a remains a subject of current investigations (Bradley et al. 2001, Gostintsev et al. 1989, Kwon et al. 2002, Sivashinsky 2002).

2.3. Nonlinear Evolution of Hydrodynamically Unstable Flames

Hydrodynamical instability leads to corrugated structures with transverse dimensions that are much larger than the typical wavelength of ordinary cellular flames and, unlike the latter, the effect does not depend on the mixture composition. Lind & Whitson (1977) performed experiments of large expanding flames using lean hydrocarbon-air mixtures in 5–10 m thin plastic hemispherical bags. The bag tore loose at the early stage of propagation leaving the flame to expand freely at a nearly constant pressure. The expanding flame first appeared as a blue hemisphere, but as its size increased the surface became rough with a "pebbled" appearance. The corrugations increased in size to about 0.4–1.0 m with a finer structure superimposed. The measured propagation velocities were 1.6–1.8 times the laminar flame speed. The results were nearly the same for all five fuels studied even though their normal burning velocities vary by a factor of four.

Theoretical progress on the nonlinear development of hydrodynamically unstable flames has relied primarily on simplified models of a nominally planar front. One such model is the Michelson-Sivashinsky (MS) equation, named after the authors who derived it and provided the first numerical integration (Michelson & Sivashinsky 1977, Sivashinsky 1977). The MS equation is obtained in a weakly nonlinear long-wave

asymptotic limit, valid when the density contrast across the flame is small, or $\sigma \sim 1$. There have been attempts to extend the MS model by including higher-order terms (see, for example, Bychkov 1998 and Kazakov & Liberman 2002), but these studies produced results that are practically similar to those predicted by the MS equation. Because in the weak thermal expansion limit the DL growth rate $\omega_{\mathrm{DL}} \sim \frac{1}{2}(\sigma - 1)$ is relatively small, the evolution is described on the slow timescale $\tau = (\sigma - 1)t$. For an unperturbed planar flame propagating in the negative y-direction, the perturbed front is expressed in the form $y = -S_{\mathrm{L}}t + (\sigma - 1)\varphi$, where $\varphi = \varphi(\mathbf{x}, \tau)$, and the problem reduces to a single integro-differential equation for the flame displacement φ. Let the transverse domain of integration L be used as a unit of length, S_{L} as a unit of speed, and L/S_{L} as a unit of time, the evolution equation (in dimensionless form) becomes

$$\frac{\partial \varphi}{\partial \tau} + \frac{1}{2}(\boldsymbol{\nabla}\varphi)^2 - \alpha\, \boldsymbol{\nabla}^2\varphi - \frac{1}{8\pi^2}\int |\mathbf{k}|\, \mathrm{e}^{i\mathbf{k}\cdot(\mathbf{x}-\tilde{\mathbf{x}})}\, \varphi(\tilde{\mathbf{x}}, \tau)\, \mathrm{d}\mathbf{k}\, \mathrm{d}\tilde{\mathbf{x}} = 0.$$

When linearized, this equation yields the dispersion relation (Equation 3) expanded to $\mathcal{O}(\sigma - 1)$, where α, which is proportional to $Le_{\mathrm{eff}} - Le^*_{\mathrm{eff}}$ and inversely proportional to L, is the reduced Markstein number.

The MS equation admits exact solutions that correspond to cusp-like structures (or cells) extended periodically in transverse directions that propagate at a constant speed along the y-axis without changing shape. On a finite domain $0 \le x \le 1$ with periodic boundary conditions the cusp-like solution takes the form $\varphi = -U\tau + \Phi(x)$ with $U = \frac{1}{2}\int_0^1 \Phi_x^2\, \mathrm{d}x$. Hence, the fractional increase in propagation speed U is equal to the fractional increase in surface area of the flame front. Of particular interest is the set of so-called coalescent pole solutions, $\Phi_N(x)$, obtained as a finite sum from contribution of N-poles whose (common) real parts represent the location of the "cusp" and imaginary parts their heights (Thual et al. 1985). The propagation speed of the N-pole solution, $U_N = 2\pi N\alpha(1 - 4\pi N\alpha)$, increases when reducing α and asymptotes to a constant value $U_\infty = 1/8$ as $\alpha \to 0$. The stability results of (Vaynblat & Matalon 2000a,b) show that for any value of $\alpha > 0$ there exists, among the family of coalescent pole solutions, one and only one asymptotically stable solution. This implies that for any value of $\alpha > 0$, the long-time behavior of the solution of the MS equation, starting with arbitrary initial data, would converge to a steady propagating pole solution.

Numerical experiments show that when α is not too small the short wavelength corrugations introduced through initial disturbances merge, forming bigger cells as time progresses. These eventually coalesce into a single-peak structure filling up the entire interval that propagates at a constant speed (see **Figure 3**). The solution appears to converge exactly to the corresponding pole solution (shown as the dotted red curve in the figure). No change in shape is detected when continuing the integration over a longer time interval. Thus, when the transverse cell dimension L is not too large, the cusp-like structure is stable and propagates as a whole at a constant speed that is larger than the speed of a planar flame.

The general structure of the solution is retained in computations carried out for small α, but the solution does not settle to a steadily propagating state. Rather, small random-like subwrinkles appear sporadically on the flame front and the speed of

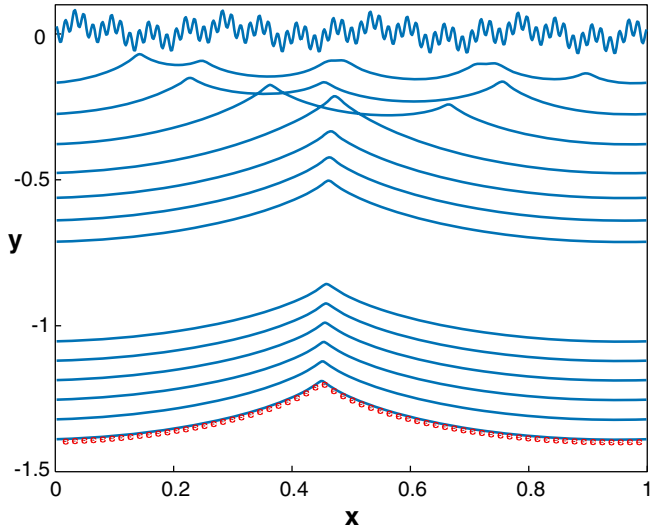

Figure 3

The development of the flame-front profile $\varphi(x, \tau)$, based on the MS equation for $\alpha = 0.005$, starting with arbitrary initial data. The flame is propagating along the negative y-axis. The small disturbances introduced through the initial conditions merge and form bigger cells that eventually coalesce into a single-peak structure. The long-time behavior of the numerical solution coincides with the exact pole solution shown as the red dotted curve.

propagation varies continuously in time. The wrinkles appear first on the troughs, propagate along the flame surface, and disappear at the crests (see **Figure 4**). In a series of numerical experiments (Rastigeyev & Matalon 2006a), it was verified that the appearance of wrinkles is highly sensitive to the level of numerical noise and to the so-called aliasing effect, where the solution gets contaminated by high-frequency modes, which appear on the discrete grid and cannot be properly distinguished from the correct lower modes. The number of wrinkles appearing on the solution was reduced significantly by increasing the numerical accuracy and/or suppressing the aliasing effect. Furthermore, small-scale wrinkles that closely resemble those emerging from the numerical noise were artificially created by introducing a low-amplitude external forcing, representing random noise on an otherwise smooth steadily propagating profile. Hence, when the transverse cell dimension L is sufficiently large, a low level of background noise provides small disturbances that are rapidly magnified by the hydrodynamic instability, resulting in small-scale wrinkles formed sporadically on the flame front. External noise may result, for example, from a weakly turbulent flow in the incoming stream. The turbulence then provides a permanent level of noise that enables the multiscale nature of the flame surface to be sustained. The appearance of wrinkles causes the flame to accelerate with the propagation speed increasing further until the wrinkles merge at the crest. The disappearance of the wrinkles is associated with a drop in propagation speed. The decrease in speed continues either until the flame stabilizes to the appropriate pole solution, or until new wrinkles reappear on the flame front (see **Figure 5**). On average, the propagation speed is significantly increased (nearly doubled) in the presence of noise. This provides a possible explanation of the unsteady pebbly-like structures observed on the front of sufficiently large flames and the associated large increase in propagation speed.

Numerical simulations of the Navier-Stokes equations, without restriction on the thermal expansion parameter, were carried out recently by Rastigeyev & Matalon

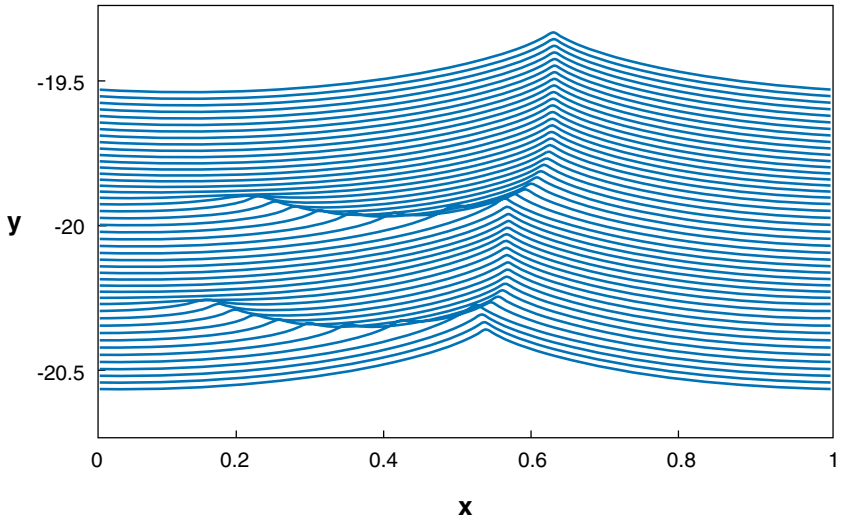

Figure 4

The development of the flame-front profile $\varphi(x, \tau)$, based on the MS equation for $\alpha = 0.004$, starting with arbitrary initial data. The flame is propagating along the negative y-axis and does not settle to a steadily propagating state. The solution is continuously contaminated by small wrinkles that appear sporadically near $x = 0$, propagate along the surface, and disappear at the crest. Although the solution seems to have reached a steady state, new wrinkles appear on the front if the integration is carried out for a longer time interval.

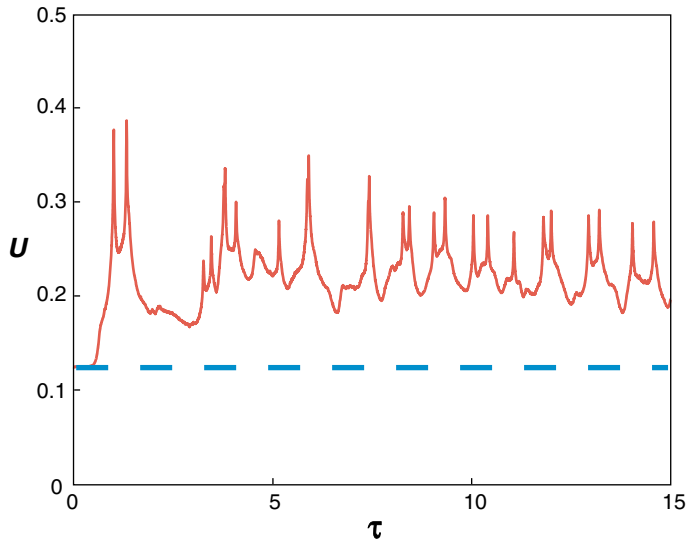

Figure 5

The increment in propagation speed (scaled appropriately) of a corrugated flame with $\alpha = 0.005$ subjected to noise as a function of time. In the absence of noise, the cusp-like structure that develops coincides with the 8-pole solution, which propagates at a constant speed $U \approx 0.124$ (*dashed blue line*). Note that the average speed is significantly increased as a result of noise.

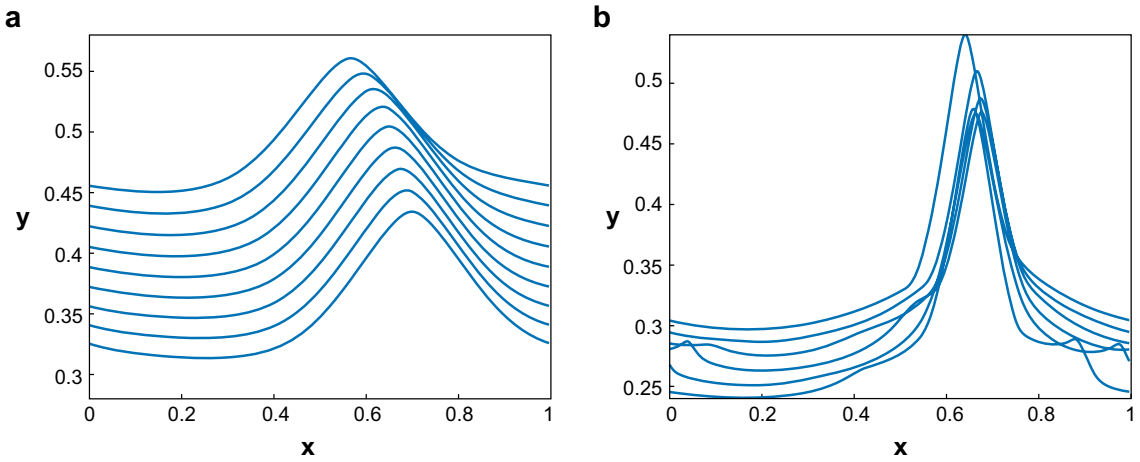

Figure 6

The development of a flame front for (*a*) $\alpha = 0.005$ and (*b*) $\alpha = 0.0005$ with a realistic $\sigma = 6$. The profiles shown in the figure correspond to the long-time behavior of the solution, after the initial transient has faded out. The flame shape shown in the figure has been scaled; for the physically correct amplitudes the graph must be amplified by a factor $\sigma - 1 = 5$.

(2006a,b) within the framework of a hydrodynamic theory. The results indicate that the predictions of the MS equation remain qualitatively correct for realistic σ. If the transverse size L is not too large, a steadily propagating single-peak structure emerges but with a significantly larger amplitude. The small-scale unsteady behavior uncovered when L is large is also similar to the MS prediction, except that for $\sigma \approx 6$ the first appearance of the small-scale wrinkles on the surface of the flame front (for a given grid resolution) occurs at a much larger value of L. **Figure 6** illustrates these two cases. The graph shows the development of φ as a function of time, after the initial transient has faded out. A smooth structure that propagates steadily results when $\alpha = 0.005$. But for $\alpha = 0.0005$ the solution never settles to a steady state; small-scale perturbations are continuously created at the troughs and travel along the front, disappearing at the crests. One also notes that as α decreases the cusp appears sharper and sharper and the "parabolic" convex part of the flame front gets flatter.

The propagation speed of the corrugated front increases with decreasing α but quickly reaches an asymptote, so that the relative increment in speed becomes independent of the mixture composition and of the lateral size L. It scales linearly with the thermal expansion coefficient, and for realistic values of σ it amounts to an increase in speed of 7–15%. The average incremental speed, however, increases significantly when noise-generated unsteady structures evolve on the surface, as illustrated in **Figure 5**, and can attain values close to twice the laminar flame speed.

The nonlinear development of a spherically expanding flame is far more complex. Although the MS equation can be extended to account for the expansion rate (Rahibe et al. 1995), the results are only valid locally and apply to a weakly curved segment of the front. Computations that apply to the whole spherical flame surface are extremely

extensive and costly even within the simplification of weak thermal expansion. With model equations it was possible to reproduce to some extent the observed complex network of wrinkles (D'Angelo et al. 2000) or the acceleration induced by the wrinkling (Karlin & Sivashinsky 2006).

In their seminal papers, Darrieus and Landau both concluded that the instability of a flame front modeled as a surface of density discontinuity leads to turbulence. Darrieus has further stated that, although the prediction of turbulence is essential and confirms the expectation of an ideal fluid, it is paradoxical that the introduction of viscosity in the calculation does not assure stability. Contrary to this view, the evidence today supports the idea that hydrodynamic instability leads to corrugated structures with relatively large transverse dimensions that propagate steadily at a speed much larger than the laminar flame speed. The larger cells are sensitive to background noise, resulting in small-scale wrinkles that appear sporadically on the flame surface, travel along the flame surface, and cause a significant increase in its average speed. The self-wrinkling phenomenon may eventually lead to turbulence.

3. NONPREMIXED COMBUSTION

Intrinsic instabilities in nonpremixed combustion have not been studied as extensively as in premixed flames. The reason may lie in the difficulties of observing such instabilities in a simple configuration that enables analytical treatment and provides means for direct comparison with experiments. Flat premixed flames can be observed in the laboratory in a carefully controlled uniform flow kept equal to the laminar flame speed. The formation of cellular structures, the onset of oscillations, and the occurrence of other complex patterns are then easily established by changing the flow conditions and/or mixture composition. In contrast, a steady planar diffusion flame in a truly one-dimensional setting is not possible. For a one-dimensional net flow rate the flux of the reactant originating at infinity and diffusing against the flow is necessarily fixed all the way down to the flame. This implies that the concentration of this reactant must remain constant so that the reactant cannot be depleted at the flame as required.

The first known instability in diffusion flames is due to Gardside & Jackson (1951), who observed that when diluted with N_2 or CO_2 the surface of a hydrogen-air jet flame often comprises triangular cells in the shape of a polyhedron. Later, Dongworth & Melvin (1976) observed that the base of a hydrogen-oxygen diffusion flame on top of a splitter-plate burner, which is normally straight, takes on a cellular appearance when the flow rate is sufficiently high and the reactants are diluted in N_2 or Ar but not in He. Chen et al. (1992) also reported the occurrence of cellular structures on slot-burner hydrocarbon-air diffusion flames diluted with SF_6 but not with N_2, CO_2, or He. Similarly, Ishizuka & Tsuji (1981) observed the formation of stripes, or elongated cells, on the surface of N_2-diluted hydrogen-oxygen counterflow diffusion flames in the unstrained cross-flow direction. The experimental record of flame oscillations, which is another form of instability, includes condensed-phase fuels (Chan & Tien 1979), candle and large suspended fuel droplets in a microgravity environment (Nayagam & Williams 1998, Ross et al. 1991), jet and spray diffusion flames (Füri et al. 2000,

Golovanevsky et al. 1999), and flame spreading over liquid beds (Ross 1994). The nature of the oscillation in each of these experiments is quite different. The droplet flame exhibits radial oscillations. The jet flame expands and contracts as a whole during a cycle. For the microgravity candle flame, the edge moves back and forth along its hemispherical surface. Similarly, in flame spreading the oscillations are primarily seen near the edge, decaying along the trailing diffusion flame.

3.1. Diffusion Flames

It is evident that the observed cellular and oscillating flames result from a diffusive-thermal instability and are not hydrodynamically driven.[3] Most theoretical studies have therefore adopted a constant-density model to filter out the hydrodynamic disturbances. The problem then reduces to a reaction-diffusion system with a prescribed flow. Although thermal expansion has a marked influence on flame instability, as discussed below, it does not play a crucial role as it does with premixed flames, which provides a posteriori justification for the constant-density assumption. Even within this framework, the problem is rather complicated because of the large number of parameters involved. These include the two Lewis numbers Le_F and Le_O associated with the fuel and oxidizer, respectively, the initial mixture strength ϕ defined as the fuel-to-oxidizer mass supplied in the respective streams normalized by their stoichiometric proportions, the difference between temperatures at the opposing boundaries, and the flow conditions characterized by a Damköhler number $\mathbb{D}$ defined as the ratio of the residence time in the flame zone to the chemical reaction time U_c. The Damköhler number is inversely proportional to the square of the characteristic speed U_c.

The underlying hydrodynamics in the reported experiments is generally nontrivial, involving multidimensional shear and strained flows that produce nonuniform conditions over the flame surface and complicate theoretical investigations even within the context of constant density. To retain one-dimensional simplicity, investigators adopted an idealized construct—the one-dimensional chambered diffusion flame—for theoretical modeling (Kirkby & Schmitz 1966, Matalon et al. 1979). The idealized burner in these studies is supplied from the bottom with fuel through a semipermeable plate, which maintains a uniform flow throughout the cross section and prevents backward diffusion of products. The other reactant, the oxidizer, diffuses uniformly from the top of the chamber assumed to be at a finite distance away, to the flame against the upward flow of products. Conditions across the top exit of the combustion chamber, where the oxidizer originates, are maintained constant by a fast-flowing stream. Lo Jacono et al. (2005) recently introduced a novel design where the difficulty of creating uniform conditions in the horizontal cross section at the top is overcome by introducing the oxidizer through an array of hundreds of closely

[3] Combustion studies that favor an unstable underlying flow, which promotes mixing, are often of interest. The influence of heat release on Kelvin-Helmholtz instability in a mixing layer, for example, was studied by Jackson & Grosch (1990) in the context of an inviscid flow with a flame-sheet approximation. Coupled hydrodynamic and combustion modes at near-extinction conditions were studied by Papas et al. (2003) using the boundary-layer equations and a parallel flow approximation. However, these studies fall outside the scope of this review.

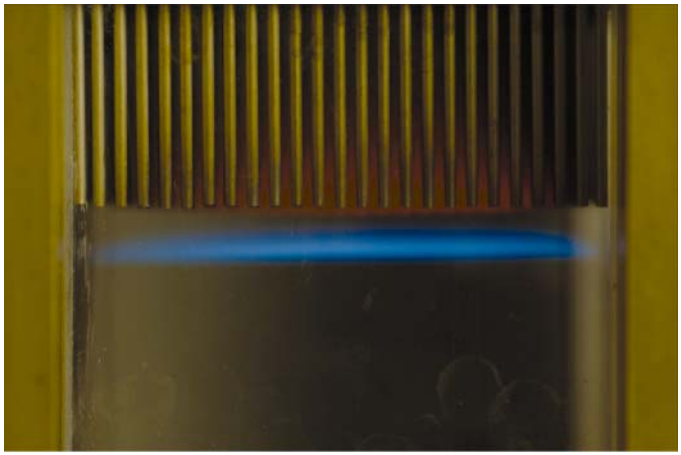

Figure 7

Photograph of a planar CO_2-diluted hydrogen-oxygen diffusion flame (*side view*) in a porous plug counter-diffusion (PPCD) burner. The needles supplying the oxidizer are seen at the top of the figure. Courtesy of P.A. Monkewitz.

spaced hypodermic needles and allowing the combustion products to escape vertically through the space between the needles. **Figure 7** shows a side-view photograph of a planar unstrained flame in what will be referred to as the porous plug counter-diffusion (PPCD) burner. Measured strain rates along the flame front were less than $1\,s^{-1}$ and are associated with flow nonuniformities resulting from heat loss to the chamber walls, which can be minimized by appropriate heat-loss management. The realization of a planar unstrained diffusion flame will likely increase the experimental data on diffusion flame instability and facilitate direct comparison with theory.

Stability analysis of diffusion flames has predominantly used a planar flame as the basic state (Cheatham & Matalon 2000, Kim 1997, Kim et al. 1996, Kukuck & Matalon 2001, Miklavcic et al. 2005, Vance et al. 2001). Although the various models differ slightly by the boundary conditions imposed, these minor differences do not affect the results in any significant way. However, because the configuration is not symmetric, interchanging the roles of fuel and oxidizer has important consequences. In general, an observer located at the flame sees a net mass flux directed either from the fuel or from the oxidizer side. Therefore, one of the reactants diffuses against the stream and has a special role in determining the location and stability of the flame. In the discussion presented below it is assumed, as in the description of the PPCD burner, that fuel is supplied in the upcoming stream and the oxidizer diffuses against the stream. For the reverse configuration—the inverse diffusion flame—the role of fuel and oxidizer must be interchanged when interpreting the results. Both setups can be tested experimentally.

The most comprehensive stability results are based on the asymptotic model proposed by Cheatham & Matalon (2000), which exploits the limit of a large activation energy, or large Zel'dovich number $\beta \gg 1$, for a one-step irreversible global chemical reaction. The chemical activity is then confined to a sheet and the formulation reduces to a nonlinear free-boundary problem for determining the temperature and reactant mass fractions as well as the instantaneous shape of the sheet itself. By resolving the reaction zone on the $\mathcal{O}(\beta^{-1})$ scale, appropriate conditions that describe the influences

of the reaction and diffusion processes are obtained as matching conditions. Unlike the fast chemistry limit, $\mathbb{D} \to \infty$, where the fuel and oxidizer are completely consumed along the stoichiometric surface as envisaged by Burke & Shumann (1928), the present theory permits incomplete combustion with different degrees of reactant consumption. It is therefore applicable to conditions that extend from complete combustion down to extinction, namely for $\mathbb{D}_{ext} \leq \mathbb{D} < \infty$, where $\mathbb{D}_{ext}$ denotes the conditions where steady burning can no longer be sustained and the flame is extinguished because of a low enough temperature and excessive reactant leakage.

The stability analysis of a planar flame yields an explicit dispersion relation, but due to its transcendental nature, finding roots for the growth rate in the complex plane requires substantial numerical computations (Cheatham & Matalon 2000, Kukuck & Matalon 2001). Therefore, results have also relied on numerically solving the free-boundary problem directly (Metzener & Matalon 2006), an approach useful in extending the analysis to account for density variations. The Burke-Schumann solution of complete combustion is unconditionally stable. Similarly, the flame for the equidiffusion case, $Le_F = Le_O = 1$, is stable for all $\mathbb{D}$. In both cases the available enthalpy at the reaction sheet $h_f = 0$, so when instabilities exist they are necessarily associated with excess or deficiency in the available enthalpy. This occurs as a result of differential—nonunity Lewis numbers—and preferential—unequal Lewis numbers—diffusion, and at high flow rates, namely when the Damköhler number is sufficiently low or $\mathbb{D}_{ext} \leq \mathbb{D} < \mathbb{D}^*$. The marginally stable state $\mathbb{D}^*$ depends on the mixture composition.

The various patterns that are likely to be observed at the onset of instability are summarized in the Lewis numbers parameter plane of **Figure 8**. The plane is divided into several regions by two curves. The solid red curve $h_f = 0$ separates regions

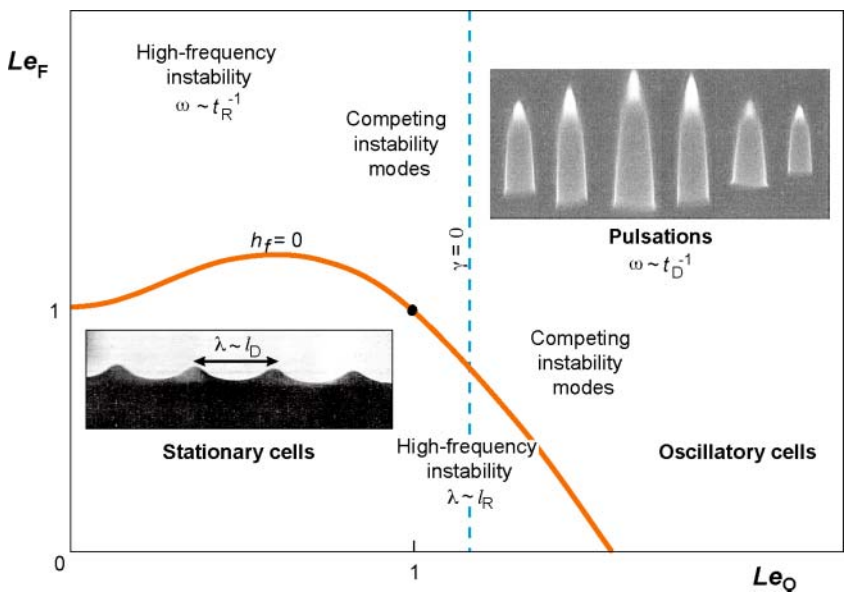

Figure 8

Diagram illustrating the various possible modes of instability in the fuel-oxidizer Lewis numbers parameter plane. The solid red curve $h_f = 0$ separates regions where there is excess (*below*) and deficiency (*above*) in available enthalpy at the reaction sheet; the dashed blue vertical line separates regions of relatively lean (*left*) and rich (*right*) mixtures.

of excess (below the curve) and deficiency (above the curve) in available enthalpy at the reaction sheet; it always includes the point $Le_F = Le_O = 1$ and stretches out as ϕ decreases to include a wider range of Le_O. The dashed blue vertical line $\gamma = 0$ separates regions of relatively lean (to the left) and rich (to the right) mixtures, and shifts to the right as the initial strength ϕ decreases.

Stationary cells are formed and sustained when the available enthalpy is in excess. This occurs primarily when the two Lewis numbers are less than one, but could also result when one of the Lewis numbers is near, or even slightly above, one, provided the other is less than one. The characteristic cell size is given by $\lambda = 2\pi/k^*$, where k^* is the wave number of the most amplified disturbance. Typical cells evolve on the diffusion time $t_D = \mathcal{D}_{th}/l_D^2$ and scale on the diffusion length $l_D \sim D_{th}/U_c$. For fuel-lean systems $k^* \approx 0.5 - 4l_D^{-1}$, which, depending on the characteristic speed, yield cells 0.3–2 cm wide. But for near stoichiometric conditions and in slightly rich mixtures the cells are much smaller, and scale on the reaction zone thickness $l_R = \beta^{-1} l_D$. Disturbances now intrude in the reaction zone and a separate analysis that incorporates small wavelength perturbations evolving on the fast time $t_R = \beta^{-2} t_D$ is required (Buckmaster et al. 1983, Kim 1997, Kim & Lee 1999). These high-frequency modes, also referred to as fast-time instabilities, are limited to conditions that are very near the extinction limit, or $\mathbb{D}^* \approx \mathbb{D}_{ext}$. In contrast, ordinary cells are predicted to occur over a wider range of flow rates, with $\mathbb{D}^* - \mathbb{D}_{ext} = \mathcal{O}(1)$, and are more likely to be observed in practice.

The transition from a planar to a cellular structure was observed experimentally in a CO_2-diluted hydrogen oxygen flame in a PPCD burner (Lo Jacono et al. 2005). The oxygen concentration injected from the hypodermic needle supply varied in the range 10.6–100% by mass. For each oxidizer mixture, the hydrogen mass fraction in the fuel stream was gradually decreased by increasing the CO_2 concentration. For an oxidizer mixture with 62.9% O_2, the flame was planar when the fuel stream contained 1.5% H_2 by mass, as shown in **Figure 7**. The spontaneous formation of cells was first observed when the H_2 concentration was reduced to approximately 1.25%. A typical cellular pattern is shown in **Figure 9**. The cellular structure was retained when reducing the hydrogen concentration down to 0.7%, but reducing it further resulted in flame

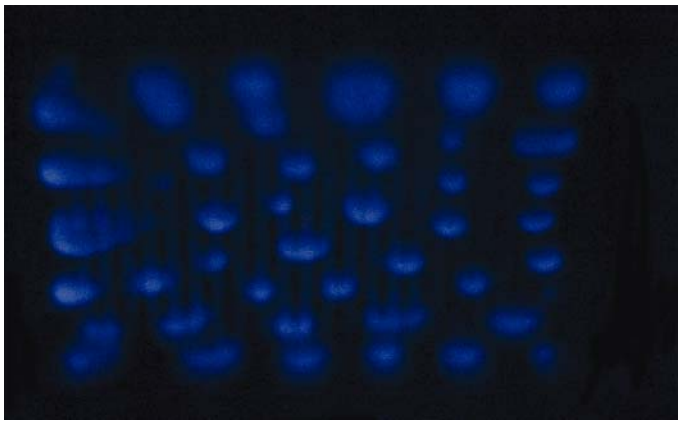

Figure 9

Photographs of a cellular CO_2-diluted hydrogen-oxygen diffusion flame, taken at an oblique angle, in a porous plug counter-diffusion (PPCD) burner. Courtesy of P.A. Monkewitz.

extinction. The observed cells during the transition were ~0.4–1 cm, with the smaller size seen near extinction. Cellular flames were observed over a significant range of H_2 concentration, corresponding to an initial mixture strength $\phi < 1$, namely in lean systems, and for conditions corresponding to $Le_O \sim 0.97$–1.33 and $Le_F \sim 0.22$–0.29. In richer systems, or $\phi > 1$, they were either observed just prior to extinction or were never observed. The conditions for the onset of the cellular instability as well as the typical dimension of the observed cells are in complete agreement with the theoretical predictions.

Cells at the base of jet flames and flames on top of slot and splitter-plate burners were observed in H_2–O_2 systems diluted in N_2 or Ar, in which case $Le_F \sim 0.33$–0.35, but not when the dilutent was He because in this case $Le_F \sim 1.02$ is too large. They were also observed in hydrocarbon-air flames when diluted in SF_6, which tends to lower the Lewis numbers significantly, but not when diluted in N_2 or CO_2. The reported cell sizes in these studies were approximately 0.7–1.5 cm. The conditions for the onset of the cellular instability appear in general agreement with the theoretical predictions even though the underlying hydrodynamics in the reported experiments is far more complex. Evidence that the typical cell size in these circumstances also depends on the transverse velocity gradient, or shear-layer thickness, was recently proposed by D. Lo Jacono & P.A. Monkewitz (unpublished manuscript).

Deficiency in enthalpy in the reaction zone leads to oscillations. When both Lewis numbers are larger than one, the fastest-growing mode is one of zero wave number so that the preferred mode of instability is planar pulsations with the flame moving back and forth in a direction perpendicular to its surface. In rich systems the frequency of oscillations scales on the inverse of the diffusion time and is estimated at 1–6 Hz (Kukuck & Matalon 2001); for lean mixtures the onset occurs near the extinction limit as a high-frequency mode that scales on the inverse of the reaction time. The onset of planar pulsations in the PPCD burner has not yet been observed, but comparison with jet diffusion flames, which contract and expand vertically during a cycle, shows that the predicted conditions are indeed commensurate with the observations (Füri et al. 2000). For example, oscillations were observed for propane-air flames diluted in nitrogen when $\phi \geq 1.32$, in which case Le_F varied from 1.1 to 1.8 with $Le_O \approx 1$, but were not observed for $\phi \leq 0.76$ despite the large-fuel Lewis number $Le_F = 1.86$, which resulted from the N_2-dilution.

While the linear theory is able to predict the onset of oscillations, the subsequent flame behavior must be determined by a nonlinear analysis. A standard bifurcation analysis carried out by Cheatham (1997, pp. 135–38) yields amplitude equations that, depending on the parameters, lead to either unbounded or time-periodic solutions. Therefore, sustained oscillations (limit cycle) can only occur in a restricted range of the parameters; otherwise the oscillations lead to premature extinction or blow off. Wang et al. (2006) recently provided a careful mapping of the parameters appearing in the amplitude equations.

Although cellular structures and flame oscillation are the predominant forms of instability, other possible patterns may exist in the transition regions between various domains or for extreme values of the parameters. Oscillating cells, for example, result when $Le_F < 1$ and Le_O is sufficiently large from competing modes of comparable

and/or disparate scales. Mixed modes of instability were noted in jet diffusion flames in the form of traveling, or rotating, cells (Lo Jacono et al. 2003), and more recently in the flat flame of the PPCD burner in the form of transverse oscillations, or traveling waves of long wavelength (P. Papas & P.A. Monkewitz, private communication).

The main consequence of nonunity Lewis numbers on the combustion field is that it yields temperature and concentration profiles that are nonsimilar. A volumetric heat-loss term that affects the temperature but not the concentration fields also generates nonsimilar profiles and thus promotes diffusive-thermal instabilities. In the presence of gas-phase radiation, for example, Cheatham & Matalon (1996) found that flame oscillation can be triggered by appreciable heat losses even for unity Lewis numbers, and the instability is enhanced by heat losses when the conditions already favor oscillations (Kukuck & Matalon 2001). Oscillations in a bandwidth of 1–3.5 Hz were observed when a fraction of the fuel supplied in a jet flame was introduced in the liquid phase in the form of droplets (Golovanevsky et al. 1999). Under similar conditions, but with the droplet's content replaced by fuel vapor, a stable flame was established. In this case, the instability is attributed to heat loss from the gas phase extracted for droplet vaporization. A complementary analysis containing the essential features of the experimental conditions confirmed the importance of heat loss in triggering flame oscillations. Further compelling evidence of the role of heat loss was provided when water droplets, instead of fuel droplets, were injected, which led to oscillations of similar frequencies.

Because thermal expansion is not the driving mechanism for instability, the general characterization described above remains qualitatively correct even when realistically accounting for density variations (P. Metzener & M. Matalon, forthcoming manuscript). Thermal expansion was found to have a different influence on the various modes of instability, and its overall effect depends on the ratio of the stoichiometric and supply temperatures $r = T_a/T_u$, as well as on the temperature differential across the entire combustion layer. For example, the degree of instability for the onset of cells increases with increasing r and the marginal stability Damköhler number $\mathbb{D}^*$ is significantly larger than the value predicted by the constant-density model. On the other hand, the degree of instability for the onset of planar pulsations decreases with increasing r, and the marginal stability Damköhler number $\mathbb{D}^*$ is smaller than the value predicted by the constant-density model. The range of conditions leading to cellular flames is therefore wider as a result of thermal expansion, whereas those leading to oscillations are more restricted.

3.2. Edge-flames

A simple configuration of an edge-flame stabilized near the trailing edge of a splitter plate separating coflowing streams of fuel and oxidizer is shown in **Figure 10**. Depending on the velocities of the fuel and oxidizer streams, the flame may be either attached to or lifted off away from the plate. The attached flame is a diffusion flame that separates a region of primarily fuel from a region where there is mainly oxidizer. But when the flame is lifted it assumes the tribrachial structure shown in the figure, which consists of lean and rich premixed segments with a diffusion flame trailing

Figure 10

Edge-flame stabilized at the trailing edge of a splitter plate separating coflowing streams of nitrogen-diluted methane and air. The flame is stabilized by a negative velocity gradient in the streamwise direction. Photograph taken by Kioni et al. (1993).

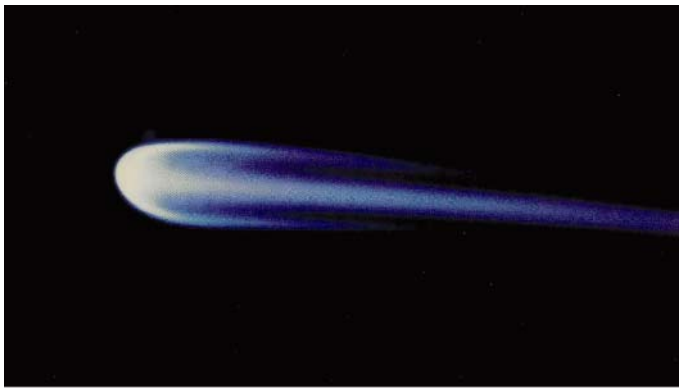

behind. The standoff distance of the edge determined by the propagation speed relative to the incoming gas depends on several parameters: the mean flow rate and the thickness of the boundary layer leaving the splitter plate, which characterize the flow conditions; the diffusivities of the reactants Le_F and Le_O and the mixture strength ϕ that characterize the mixture composition; and the ratio of the stoichiometric and supply temperatures r that characterizes the effects of the exothermicity of the reaction or thermal expansion. In the absence of preferential diffusion ($Le_F = Le_O$) and when the fuel and oxidizer are supplied in stoichiometric proportions, the edge-flame is symmetric with respect to the axis and the trailing diffusion flame remains parallel to the plate; otherwise it leans toward one of the two sides approximately along the stoichiometric surface.

Thermal expansion introduces displacement velocities proportional to S_L by the premixed flames and therefore has a significant effect on the flow field and consequently on the flame standoff distance. Nevertheless, most edge-flame calculations, and in particular stability considerations, are based on the constant-density approximation ($r = 1$), which appears to qualitatively provide the appropriate conditions for the onset of instability.

Studies of edge-flame oscillations were carried out numerically by Buckmaster and coworkers (Buckmaster 2002), who used a model problem of a flat flame along an axis, with fuel and oxidizer supplied at two opposing ends in the transverse direction. The edge results when cutting off the fuel supply at a finite position. The calculations reveal that the edge-flame oscillates back and forth along the axis when the Damköhler number is sufficiently low and the fuel Lewis number is sufficiently larger than one; the oxidizer Lewis number was assumed equal to one.

The edge-flame in a mixing layer was studied by Kurdyumov & Matalon (2002, 2004) assuming that the streams were of equal and constant velocities, and more recently (2006) using a realistically computed flow near the trailing edge of the plate. Although the boundary-layer approximation can be used to describe the mixing process between the two streams, there is a small region near the tip of the plate where the flow field must satisfy the full Navier-Stokes equations. This region is embedded in the lower of the much larger triple-deck region that describes the flow near the

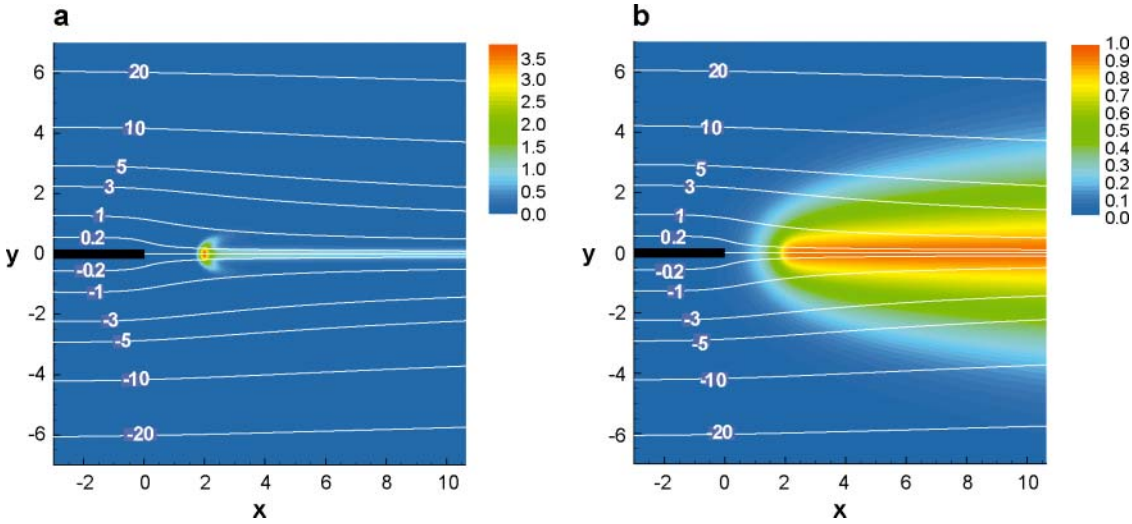

Figure 11

Edge-flame near the trailing edge of a splitter plate separating coflowing streams of fuel and oxidizer; computed for the symmetric case, $Le_F = Le_O$ with the reactants supplied in stoichiometric proportion, no heat loss, a scaled Damköhler number $\mathbb{D} = 5$, and $\beta = 10$. The white curves correspond to streamlines and the different color shades to (*a*) reaction rate contours and (*b*) isotherms, with low/high values as indicated in the legend.

plate's trailing edge, and scales as $\mathrm{Re}_{\mathrm{BL}}^{-1/2}$, where $\mathrm{Re}_{\mathrm{BL}}$ is the Reynolds number based on the thickness of the boundary layers along the plate. Results of computations for the symmetric case in the absence of heat loss are shown in **Figure 11**. The flow pattern illustrated by selected streamlines shows the entrainment of fuel and oxidizer into the mixing layer. The change in the streamlines slope at the downstream edge of the boundary layer corresponds to an acceleration experienced by the fluid elements while crossing the section $x = 0$. The lifted flame and its tribrachial nature are clearly seen in the two graphs, where appropriately scaled reaction-rate contours and isotherms are drawn. The standoff distance depends primarily on the Damköhler number $\mathbb{D}$, which is inversely proportional to the characteristic flow rate, and to a lesser extent on the mixture composition and the mobility of the reactants. When radiative losses are accounted for, the trailing diffusion flame is of finite extent and the standoff distance also depends on the heat-loss parameter b—the ratio of the radiative heat loss to the chemical energy release.

The dependence of the flame standoff distance on the parameters $\mathbb{D}$ and b is shown in **Figure 12** for a wide range of Lewis numbers. The standoff distance x_w is defined as the location where the reaction rate reaches its maximum value. **Figure 12*a*** shows the dependence on $\mathbb{D}$ for the adiabatic case ($b = 0$). For large $\mathbb{D}$ the flame is attached to the plate; it lifts off when increasing the flow rate, or decreasing $\mathbb{D}$, and moves away from the plate. For sufficiently small values of Le (below approximately 1.2) the solution is multivalued. In this case, marginal stability coincides with the turning point $\mathbb{D} = \mathbb{D}_{\mathrm{ext}}$,

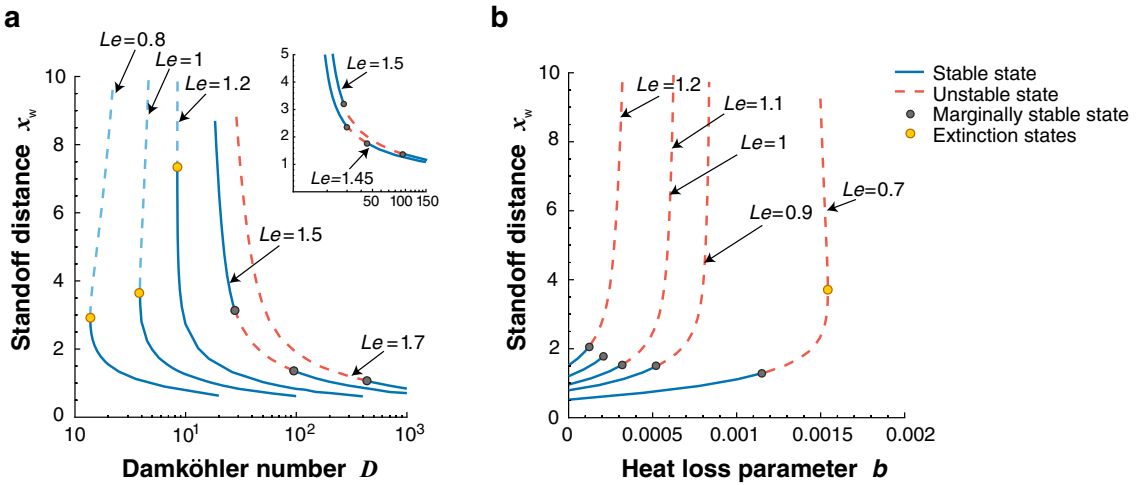

Figure 12

Response curves showing the dependence of the flame standoff distance x_w on (*a*) the Damköhler number $\mathbb{D}$ for the adiabatic case $b = 0$, and (*b*) the heat-loss parameter b for a fixed value of $\mathbb{D}$. The various curves correspond to distinct values of equal Lewis numbers, $Le \equiv Le_F = Le_O$, with the reactants supplied in stoichiometric proportions.

with the solution corresponding to the larger value of x_w unstable. An edge-flame can be stabilized near the plate only for flow rates corresponding to $\mathbb{D}_{ext} < \mathbb{D} < \infty$; for lower values of $\mathbb{D}$ it is blown off by the flow. For larger values of Le (above approximately 1.4), the solution, within the computational domain, is monotonic. The edge-flame, however, cannot always be stabilized near the plate. There is a range of unstable states corresponding to $\mathbb{D}_* < \mathbb{D} < \mathbb{D}^*$ (the marginal states are marked in the figure by black-filled circles •) where the flame undergoes spontaneous oscillations with the edge moving back and forth along the axis and dragging the trailing diffusion flame behind it. The oscillations along the sheet are weakened downstream and are completely damped at sufficiently large distances. When the combustion field is nonsymmetric, the edge of the flame is characterized by two coordinates x_w and y_w. In this case, oscillations are associated with both coordinates varying periodically in time, and the edge-flame moves back and forth along a surface that coincides approximately with the stoichiometric surface (Kurdyumov & Matalon 2004). The dependence of x_w on the heat-loss parameter b is shown in **Figure 12*b*** for a specified value of $\mathbb{D}$. Although the standoff distance x_w increases with increasing b, the flame can be stabilized near the tip of the plate only when heat losses are relatively small. When appreciable, or $b > b_c$, the flame undergoes spontaneous oscillations. The critical value b_c increases with decreasing Le and precedes the turning point (marked by a circle ○) even for Le below one. Hence, radiative losses could trigger flame oscillations and this would occur even when the Lewis numbers are equal to, or slightly less than, unity.

This discussion has centered around oscillations resulting from diffusive-thermal instabilities. Experimentally observed oscillations that occur in complex situations

may be driven by more than one factor. They have often been associated with buoyancy effects (Won et al. 2002), and for flame spread over liquid beds to the gas-phase circulation created ahead of the flame (Schiller et al. 1996) or to Marangoni instability (Higuera & Garcia-Ybarra 1998). Edge-flames may also occur in premixed systems displaying various forms of instabilities including cellular structures, as discussed by Buckmaster (2002).

ACKNOWLEDGMENTS

The work discussed in this paper has been supported by the programs of Applied Mathematics and Combustion and Plasma Systems of the National Science foundation, by NASA's Microgravity Combustion research program, and by the U.S.-Israel Bi-National Science Foundation. The hospitality of Barry J. Greenberg and the Faculty of Aerospace Engineering at the Technion - Israel Institute of Technology, under a Lady Davis Fellowship, during which part of this work was completed, is greatly appreciated. The paper has benefited from invaluable discussions with many colleagues, in particular John K. Bechtold, Barry J. Greenberg, Vadim Kurdyumov, Chung K. Law, Philippe Metzener, Peter A. Monkewitz, Paul Papas, and Grisha I. Sivashinsky, to whom I am extremely grateful.

LITERATURE CITED

Addabbo R, Bechtold JK, Matalon M. 2002. Wrinkling of spherically expanding flames. *Proc. Combust. Inst*. 29:1527–35

Bechtold JK, Cui C, Matalon M. 2004. The role of radiative losses in self-extinguishing and self-wrinkling flames. *Proc. Combust. Inst*. 30:177–84

Bechtold JK, Matalon M. 1987. Hydrodynamic and diffusion effects on the stability of spherically expanding flames. *Combust. Flame* 67:77–90

Blackshear JI, Mapp JW, Gorman M. 1984. An experimental study of pulsating low-pressure flames. *Combust. Sci. Technol*. 35:311–15

Bradley D, Cresswell TM, Puttock JS. 2001. Flame acceleration due to flame-induced instabilities in large-scale explosions. *Combust. Flame* 124:551–59

Bradley D, Harper CM. 1994. The development of instabilities in laminar explosion flames. *Combust. Flame* 99:562

Bradley D, Hicks RA, Lawes M, Sheppard CGW, Woolley R. 1998. The measurement of laminar burning velocities and Markstein numbers for iso-octaine-air and iso-octane-n-heptane-air mixtures at elevated temperatures and pressures in an explosion bomb. *Combust. Flame* 115:126

Bradley D, Sheppard CGW, Woolley R, Greenhalgh DA, Lockett RD. 2000. The development and structure of flame instabilities and cellularity at low Markstein numbers in explosions. *Combust. Flame* 122:195

Buckmaster J. 1993. The structure and stability of laminar flames. *Annu. Rev. Fluid Mech*. 25:21–53

Buckmaster J. 2002. Edge-flames. *Prog. Energy Combust. Sci*. 28:435–75

Buckmaster J, Nachman A, Taliaferro S. 1983. The fast-time instability of diffusion flames. *Physica D* 9:408–24

Burke SP, Schumann TEW. 1928. Diffusion flames. *Ind. Eng. Chem*. 20:998

Bychkov V. 1998. Nonlinear equation for a curved stationary flame and the flame velocity. *Phys. Fluids* 10:2091–98

Chan W, Tien JS. 1979. An experiment on spontaneous flame oscillation prior to extinction. *Combust. Sci. Technol*. 18:139–43

Cheatham S. 1997. *On the structure and stability of diffusion flames*. PhD thesis. Northwest. Univ., Evanston. 143 pp.

Cheatham S, Matalon M. 1996. Heat loss and lewis number effects on the onset of oscillations in diffusion flame. *Proc. Combust. Inst*. 26:1063–1070

Cheatham S, Matalon M. 2000. A general asymptotic theory of diffusion flames with application to cellular instability. *J. Fluid Mech*. 414:105–44

Chen R, Mitchell GB, Ronney PD. 1992. Diffusive-thermal instability and flame extinction in nonpremixed combustion. *24th Int. Symp. Combustion*, pp. 213–21. Pittsburgh: Combust. Inst.

Class AG, Matkowsky BJ, Klimenko AY. 2003. Stability of planar flames as gasdynamic discontinuities. *J. Fluid Mech*. 491:51–63

Clavin P. 1994. Premixed combustion and gasdynamics. *Annu. Rev. Fluid Mech*. 26:321–52

Clavin P, Williams FA. 1982. Effects of molecular diffusion and thermal expansion on the structure and dynamics of premixed flames in turbulent flows of large scales and low intensity. *J. Fluid Mech*. 116:251–82

D'Angelo Y, Joulin G, Boury G. 2000. On model evolution equations for the whole surface of three-dimensional expanding wrinkled premixed flames. *Combust. Theory Model*. 4(3):317–38

Darrieus G. 1938. Propagation d'un front de flamme. *Presented at La Technique Moderne (Paris) and in 1945 at Congrès de Mécanique Appliquée (Paris)*

Dongworth MR, Melvin A. 1976. The transition to instability in a steady hydrogen-oxygen diffusion flame. *Combust. Sci. Technol*. 14:177–82

Eteng E, Ludford GSS, Matalon M. 1986. Displacement effects of a flame in a stagnation-point flow. *Phys. Fluids* 29(7):2172–80

Frankel ML, Sivashinsky GI. 1982. The effect of viscosity on the hydrodynamic stability of a plane flame front. *Combustion Sci. Technol*. 29:207–24

Füri M, Papas P, Monkewitz PA. 2000. Nonpremixed jet flame pulsations near extinction. *Proc. Combust. Inst*. 28:831–38

Gardside JE, Jackson B. 1951. Polyhedral diffusion flames. *Nature* 168:1085

Golovanevsky B, Levy Y, Greenberg JB, Matalon M. 1999. On the oscillatory behavior of laminar spray diffusion flames: experiment and theory. *Combust. Flame* 117:373–83

Gostintsev YA, Istratov AG, Shulenin YV. 1989. Self-similiar propagation of a free turbulent flame in mixed gas mixtures. *Combust. Explos. Shock Waves* 24:563–69

Groff EG. 1982. The cellular nature of confined spherical propane-air flames. *Combust. Flame* 48:51–62

Higuera HJ, Garcia-Ybarra PL. 1998. Steady and oscillatory flame spread over liquid fuels. *Combust. Theory Model*. 2:43

Ishizuka S, Tsuji H. 1981. An experimental study of effect of inert gases on extinction of laminar diffusion flames. *18th Int. Symp. Combust.*, pp. 695–703 Pittsburgh: Combust. Inst.

Istratov AG, Librovich VB. 1969. On the stability of gasdynamic discontinuities associated with chemical reactions; the case of a spherical flame. *Astronaut. Acta* 14:453–67

Jackson TL, Grosch CE. 1990. Inviscid spatial stability of a compressible mixing layer: Part II. The flame sheet model. *J. Fluid Mech.* 217:391–420

Jackson TL, Kapila AK. 1986. Effects of thermal expansion on the stability of plane, freely propagating flames: Part II. Incorporation of gravity and heat loss. *Combust. Sci. Technol.* 49:305–17

Jomaas G, Law CK, Bechtold JK. 2005. On transition to cellularity in expanding spherical flames: experiment and theoretical comparison. *Tech. Rep. AIAA 2005–0713, 43rd ASM Meet. Exhib., Reno, NV*

Joulin G, Clavin P. 1979. Linear stability analysis of nonadiabatic flames: Diffusional-thermal model. *Combust. Flame* 35:139–53

Kadowaki S, Hasegawa T. 2005. Numerical simulation of dynamics of premixed flames: Flame instability and vortes-flame interaction. *Prog. Energy Combust. Sci.* 31:193–241

Karlin V, Sivashinsky GI. 2006. The rate of expansion of spherical flames. *Combust. Theory Model.* 10:625–38

Kazakov KA, Liberman MA. 2002. Nonlinear equation for curved stationary flames. *Phys. Fluids* 14:1166–81

Kim JS. 1997. Linear analysis of diffusional-thermal instability in diffusion flames with lewis numbers close to unity. *Combust. Theory Model.* 1:13–40

Kim JS, Lee SR. 1999. Diffusional-thermal instability in strained diffusion flames with unequal lewis numbers. *Combust. Theory Model.* 3:122–43

Kim JS, Williams FA, Ronney PD. 1996. Diffusional-thermal instability of diffusion flames. *J. Fluid Mech.* 327:273–301

Kioni PN, Rogg B, Bray KNC, Linan A. 1993. Flame spread in laminar mixing layers: The triple flame. *Combust. Flame* 95:276–90

Kirkby LL, Schmitz RA. 1966. An analytical study of the stability of a laminar diffusion flame. *Combust. Flame* 10:205–20

Kukuck S, Matalon M. 2001. The onset of oscillations in diffusion flames. *Combust. Theory Model.* 5:217–40

Kurdyumov V, Matalon M. 2002. Radiation losses as a driving mechanism for flame oscillations. *Proc. Combust. Inst.* 29:45–52

Kurdyumov V, Matalon M. 2004. Dynamics of an edge-flame in a mixing layer. *Combust. Flame* 139:329–39

Kurdyumov V, Matalon M. 2006. Stabilization and onset of oscillation of an edge-flame in the near-wake of a fuel injector. *Proc. Combust. Inst.* 31:In press

Kwon OC, Rozenchan G, Law CK. 2002. Cellular instabilities and self-acceleration of outwardly propagating spherical flames. *Proc. Combust. Inst.* 29:1775–83

Landau LD. 1944. On the theory of slow combustion. *Acta Physicochim. USSR* 19:77–85

Law CK. 2006. Propagation, structure, and limit phenomena of laminar flames at elevated pressures. *Combust. Sci. Technol.* 178:335–60

Law CK, Jomaas G, Bechtold JK. 2005. Cellular instabilities of expanding hydrogen/propane spherical flames at elevated pressures:theory and experiment. *Proc. Combust. Inst.* 30:159–67

Lind CD, Whitson JC. 1977. Explosion hazards associated with spills of large quantities of hazardeous materials. *Tech. Rep. CG-D-85-77, Dept. Transp., U.S. Coast Guard Final Rep., ADA 047585*

Lo Jacono D, Papas P, Matalon M, Monkewitz PA. 2005. An experimental realization of an unstrained planar diffusion flame. *Proc. Combust. Inst.* 30:501–9

Lo Jacono D, Papas P, Monkewitz PA. 2003. On the formation of cellular instabilities in non-premixed jet flames. *Combust. Theory Model.* 7:634–44

Mallard E, Le Chatelier HL. 1883. Combustion des mélanges gazeux explosifs. *Ann. Mines* 4:274–388

Manton J, von Elbe G, Lewis BJ. 1952. Nonisotropic propagation of combustion waves in explosive gas mixtures and the development of cellular flames. *J. Chem. Phys.* 20:153–57

Markstein GH. 1964. *Nonsteady Flame Propagation*. New York: Macmillan

Matalon M. 1983. On flame stretch. *Combust. Sci. Technol.* 31:169–81

Matalon M, Cui C, Bechtold JK. 2003. Hydrodynamic theory of premixed flames: Effects of stoichiometry, variable transport coefficients and arbitrary reaction orders. *J. Fluid Mech.* 487:179–210

Matalon M, Ludford GSS, Buckmaster J. 1979. Diffusion flames in a chamber. *Acta Astronaut.* 6:943–59

Matalon M, Matkowsky BJ. 1982. Flames as gas-dynamic discontinuities. *J. Fluid Mech.* 124:239–59

Matalon M, Matkowsky BJ. 1984. On the stability of plane and curved flames. *SIAM J. Appl. Math.* 44:327–43

Metzener P, Matalon M. 2006. Diffusive-thermal isntabilities of diffusion flames: onset of cells and oscillations. *Combust. Theory Model.* 10:701–25

Michelson DM, Sivashinsky GI. 1977. Nonlinear analysis of hydrodynamic instability in laminar flames. II. Numerical experiments. *Acta Astronaut.* 4:1207–21

Miklavcic M, Moore AB, Wichman IS. 2005. Oscillations and island evolution in radiating diffusion fames. *Combust. Theory Model.* 9:403–16

Nayagam V, Williams FA. 1998. Dynamics of diffusion flame oscillations prior to extinction during low gravity droplet combustion. *7th Int. Conf. Numer. Combust., York, UK, April*

Palm-Leis A, Strehow RA. 1969. On the propagation of turbulent flames. *Combust. Flame* 13:111–19

Papas P, Rais RM, Monkewitz PA, Tomboulides AG. 2003. Instabilities of diffusion flames near extinction. *Combust. Theory Model.* 7:603–33

Pelce P, Clavin P. 1982. Influence of hydrodynamics and diffusion upon the stability limits of laminar premixed flames. *J. Fluid Mech.* 124:219–37

Rahibe M, Aubry N, Sivashinsky GI, Lima R. 1995. Formation of wrinkles in outwardly propagating flames. *Phys. Rev. E* 52:3675–86

Rastigeyev Y, Matalon M. 2006a. Nonlinear evolution of hydrodynamically unstable premixed flames. *J. Fluid Mech.* 554:371–92
Rastigeyev Y, Matalon M. 2006b. Numerical simulations of flames as gasdynamic discontinuities. *Combust. Theory Model.* 10:459–81
Ross HD. 1994. Ignition of and flame spread over laboratory-scale pools of pure liquid fuels. *Prog. Energy Combust. Sci.* 20(1):17–64
Ross HD, Sotos RG, T'ien JS. 1991. Observations of candle flames under various atmospheres in microgravity. *Combust. Sci. Technol.* 75:155–60
Sattler SS, Knaus DA, Gouldin FC. 2002. Determination of three-dimensional flamelet orientation distributions in turbulent v-flames from two-dimensional image data. *Proc. Combust. Inst.* 29:1785–92
Schiller DN, Ross HD, Sirignano WA. 1996. Computational analysis of flame spread across alcohol pools. *Combust. Sci. Technol.* 118:203–55
Simon DM, Wong EL. 1953. Burning velocity measurement. *J. Chem. Phys.* 21:936
Sivashinsky GI. 1977. Nonlinear analysis of hydrodynamic instability in laminar flames: I. derivation of basic equations. *Acta Astronaut.* 4:1177–1206
Sivashinsky GI. 1983. Instabilities, pattern formation, and turbulence in flames. *Annu. Rev. Fluid Mech.* 15:179–99
Sivashinsky GI. 2002. Some developments in premixed combustion modeling. *Proc. Combust. Inst.* 29:1737–61
Strehlow RA. 1984. *Combustion Fundamental.* New York: McGraw-Hill
Thual O, Frisch U, Hénon M. 1985. Application of pole decomposition to an equation governing the dynamics of wrinkled fronts. *J. Phys.* 46(9):1485–94
Uberoi MS, Kuethe AM, Menkes HR. 1958. Flow field of a bunsen flame. *Phys. Fluids* 1(2):150–58
Vance R, Miklavcic M, Wichman IS. 2001. On stability of one-dimensional diffusion fames. *Combust. Theory Model.* 5:147–62
Vaynblat D, Matalon M. 2000a. Stability of pole solutions for planar propagating flames: I. Exact eigenvalues and eigenfunctions. *SIAM J. Appl. Math.* 60(2):679–702
Vaynblat D, Matalon M. 2000b. Stability of pole solutions for planar propagating flames: II. Properties of eigenvalues/eigenfunctions and implications to stability. *SIAM J. Appl. Math.* 60(2):702–28
Wang HY, Bechtold JK, Law CK. 2006. Nonlinear oscillations in diffusion flames. *Combust. Flame* 145:376–89
Won SH, Kim J, Shin MK, Chung SH, Fujita O, et al. 2002. Normal and microgravity experiment of oscillating lifted flames in coflow. *Proc. Combust. Inst.* 29(1):37–44